IOPscience iopscience.iop.org

Home Search Collections Journals About Contact us My IOPscience

A pseudopotential total energy study of impurity-promoted intergranular embrittlement

This article has been downloaded from IOPscience. Please scroll down to see the full text article.

1990 J. Phys.: Condens. Matter 2 351

(http://iopscience.iop.org/0953-8984/2/2/011)

View the table of contents for this issue, or go to the journal homepage for more

Download details:
IP Address: 171.66.16.96
The article was downloaded on 10/05/2010 at 21:25

Please note that terms and conditions apply.

J. Phys.: Condens. Matter 2 (1990) 351–365. Printed in the UK

A pseudopotential total energy study of impurity-promoted intergranular embrittlement

L Goodwin†, R J Needs and Volker Heine
Cavendish Laboratory, Madingley Road, Cambridge CB3 0HE, UK

Received 23 June 1989

Abstract. We discuss the decohesion and bond mobility models of impurity-promoted intergranular embrittlement. Both of these models are tested quantitatively using pseudopotential total energy techniques within the local density approximation. Our energy calculations are for a highly simplified 'grain boundary' consisting of substitutional germanium or arsenic impurities in a crystalline aluminium lattice. We find that the germanium and arsenic impurities increase the ideal work of fracture for creating a [111] surface by up to approximately 8%. This result is inconsistent with the decohesion model of embrittlement. We also find that both impurities substantially increase the critical shear stress (by 25% for germanium and 58% for arsenic) and that arsenic impurities decrease the cleavage stress by 14%. All our results are consistent with the bond mobility model of intergranular embrittlement.

1. Introduction

In this paper we present a pseudopotential total energy study of two very different models of impurity-promoted intergranular embrittlement; the so-called decohesion and bond mobility models. Brief reports of some of this work have already appeared elsewhere (Goodwin *et al* 1988, 1989).

For an overview of the physics of fracture, including theoretical work on embrittlement, the reader is referred to the review article by Thomson (1986). Embrittlement, despite its technological importance, remains poorly understood. This is undoubtedly due, in part, to the immense computing resources that are required for the accurate modelling of inter-atomic interactions. At present it is impossible, using a fully quantum mechanical scheme, to model a realistic fracture at an impurity-embrittled grain boundary. In addition to the computational cost, grain boundaries and the various processes associated with grain boundary fracture are exceedingly complex. As a result it is extremely difficult to sift out the essential features of the embrittlement mechanism, or mechanisms. Our approach has been to investigate the influence of particular factors in isolation by performing accurate quantum mechanical calculations on highly simplified grain boundary structures containing impurity atoms.

Attempts have been made to model the problem within a quantum mechanical scheme by simplifying the atomic structure around a segregated impurity. One of the first such approaches was to represent the grain boundary structure by a small cluster of atoms, consisting of a single impurity atom surrounded by a single shell of metal atoms.

† Present address: Department of Mathematics, Imperial College, Queen's Gate, London, SW7 2BZ, UK.

0953-8984/90/020351 + 15 $02.50 © 1990 IOP Publishing Ltd

The changes in the charge density due to the inclusion of an impurity were calculated by Briant and Messmer (1980) and Messmer and Briant (1982) and the energy to dilate such a cluster uniformly was calculated by Painter and Averill (1987). A somewhat different approach was adopted by Sayers (1984), who used a tight-binding method and included the surrounding metallic environment within a second moment approximation. The results of these calculations, and of others, have suggested that impurity-promoted integranular embrittlement results from either a weakening of the bonds across the grain boundary, with an associated reduction in the ideal work of fracture (the decohesion model), or from a reduction in the ease of atomic rearrangement around the embrittling impurity (the bond mobility model), or possibly from a combination of these two effects.

In this work we have examined the decohesion and bond mobility models of embrittlement by studying the response to applied tensile and shear strains of a dilute layer of embrittling impurities segregated in a fully three dimensional metallic environment. Aluminium was chosen for the host metal, with embrittling impurities represented by the elements arsenic and germanium. The detailed reasoning behind this choice of elements is given in section V. Firstly we calculated the fracture energies for the pure and impurity-doped metal, with the fracture occurring both at the impurity-doped layer and one layer into the metal on either side. We found in each case, for both arsenic and germanium atoms, that the presence of the impurities increased the fracture energies. We then introduced a simple crack at the impurity-doped layer and, by calculating the energy as a function of the crack width, found that the arsenic impurities made cleavage easier by decreasing the maximum sustainable tensile stress. Lastly, we applied a simple shear to our system, for both the pure and impurity-doped metal, and found that both impurities significantly increased both the maximum sustainable shear stress, and the associated energy barrier. The results of our calculations show that the decohesion model of impurity-promoted intergranular embrittlement does not correctly describe the bonding between the impurity and the metal in our system. However, our results are consistent with the bond mobility model of embrittlement.

For the calculations we used the pseudopotential total energy technique, a recent and highly accurate method of calculating structural energies. This method has been extensively applied to both metallic and insulating systems with, in general, excellent agreement with experimental results. Examples of its use include the calculation of phonon frequencies, elastic constants, phase transition pressures, phase transition temperatures, defect energetics, surface reconstructions, grain boundary structures and the structure of amorphous and liquid systems. For a review of this technique and applications of it we refer the reader to the recent article by Ihm (1988).

This paper is laid out as follows. The role of cleavage and shear processes at a crack tip in determining whether brittle or ductile fracture occurs is described briefly in section 2. The decohesion model is discussed in section 3 and the bond mobility model is discussed in section 4. In section 5 the atomic model used for testing the embrittlement models is described. Section 6 describes the total energy pseudopotential method. The cleavage calculations and results are presented in section 7 and those for shear are presented in section 8. Conclusions are drawn in section 9 and briefly summarised in section 10.

2. Cleavage and shear processes at a crack tip

It is generally through that both cleavage and shear processes are important in determining whether brittle or ductile fracture occurs in real materials. It has been suggested

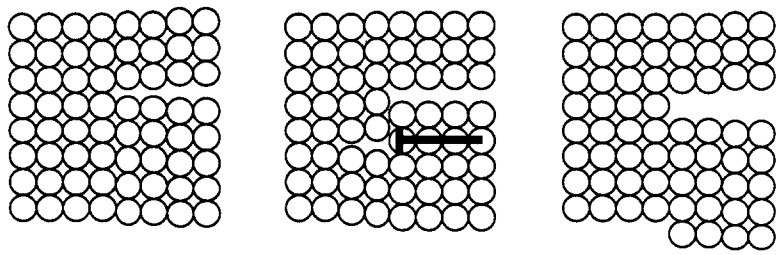

Figure 1. A schematic representation of the emission of an edge dislocation from a crack tip (after Rice and Thomson (1974)). This process reduces localised stress by blunting the crack tip.

that whether a material is brittle or ductile depends on the competition between the cleavage and shear processes at a crack tip. Crudely speaking, if cleavage is made easier then a crack is more likely to propagate, and conversely if shear processes are made easier then a crack is more likely to blunt. This basic idea was developed by Kelly, Tyson and Cottrell (1967), who, by using classical models to represent the material, were able to correctly identify the fracture trends across a wide range of materials, for example sodium chloride and diamond (brittle) and copper and gold (ductile). Later Rice and Thomson (1974) extended the model to account for the blunting at a crack tip by allowing for dislocation emission. We have illustrated the mechanism proposed by Rice and Thomson schematically in figure 1. The most interesting point to note is that the emission of an edge dislocation leads directly to blunting of the crack tip, and a reduction in the localised stresses. Figure 1 also illustrates that the process is essentially one of atomic rearrangement in which atoms slide over one another.

To make fracture and embrittlement accessible to study we reduced the problem down to what we considered to be the two fundamental and opposing processes: the ease of breaking bonds, and the ease of rearranging atoms. An ideally brittle crack propagates via the rupturing of bonds in the plane of the crack, whereas crack blunting involves dislocation emission, which in turn involves the sliding of atoms over each other. The ease of bond breaking is conceptually a straightforward quantity which can be calculated by fracturing the material. The ease of atomic rearrangement is a less straightforward quantity. We suggest that the ease of atomic rearrangement can be calculated by applying a simple shear to the sample. In later sections we shall describe calculations of fracture and simple shear, from which we shall infer the changes in the ease of bond breaking and the ease of atomic rearrangement due to the presence of impurities, and hence the change in the brittle-ductile character of the system. The central assumption is that the ease of brittle fracture, and ease of dislocation emission, can be inferred from highly idealised calculations. The logic behind this is of course open to question. The main criticisms are that our calculations do not consider dislocations explicitly, and neither do they include the detailed geometry of the crack tip. Because of this the magnitudes of the quantities that we have calculated cannot be compared directly with experimental results. While such criticisms are undoubtedly valid, and should be borne in mind, we do believe that calculations of the type we have performed can provide interesting and relevant information on the effects of embrittling impurities.

3. The decohesion model of intergranular embrittlement

In this section we describe the widely quoted decohesion model of impurity-promoted intergranular embrittlement.

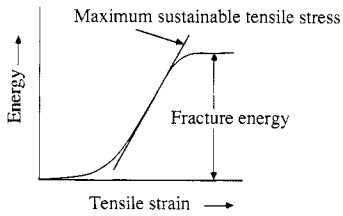

Figure 2. Energy versus tensile strain curve for a sample undergoing fracture. The fracture energy and the maximum sustainable tensile stress are indicated.

The decohesion model of embrittlement accounts for the embrittling effect of certain segregated impurities by assuming that they weaken the atomic bonds across the grain boundary (Troiano 1960, Losch 1979). This leads to reduced fracture energies and fracture stresses. The fundamental idea behind the model is that the fracture energy and the fracture stress, i.e. the maximum sustainable tensile stress, are directly correlated. In figure 2 we depict the variation of the energy as a function of the extension for a sample of metal in which a crack is opening. The maximum slope of the energy versus tensile strain curve, and the fracture energy, are marked and while it is clear that these quantities need not necessarily be related it does seem plausible that a decrease in the fracture energy will lead to a decrease in the maximum slope of the curve. A decrease in the maximum slope would then correspond to embrittlement of the material.

The first decohesion model of embrittlement (Troiano 1960) assumed that embrittlement was due to the formation of weak metal-impurity bonds. Losch (1979), recognising that the covalent bonding between a typical embrittling impurity and the surrounding metal would be very strong, proposed that it was the nearby metal–metal bonds which were weakened by the presence of the embrittling impurities. Some support has been given to this suggestion by the results of calculations, briefly referred to in section I, by Briant and Messmer (Briant and Messmer 1980, Messmer and Briant 1982), and Sayers (1984). Briant and Messmer used the so-called self-consistent field X_α scattered wave method to calculate the change in the charge distribution induced by placing an interstitial impurity atom at the centre of small clusters of nickel and iron atoms. They found that some impurities reduced the amount of electronic charge in the metal–metal bonds and increased the charge in the metal-impurity bonds. This effect was especially large in the case of sulphur, a strong embrittler, in nickel. When a boron atom was put at the centre of the cluster the charge density in the nearby nickel–nickel bonds was not reduced. As boron is an intergranular coherer, and sulphur an embrittler, of nickel, Briant and Messmer concluded that the embrittling effect of the sulphur atom was to weaken the nearby metal–metal bonds by withdrawing charge from them. Cleavage would then take place by breaking the weakened metal–metal bonds. The potency of an embrittling atom could then be measured by the amount that its electronegativity exceeded that of the host metal, which would indicate the tendency of the impurity to draw charge towards itself from the surrounding metal. This is consistent with the observation that, generally speaking, impurities with higher electronegativities are more potent embrittlers. Sayers (1984) investigated the effect of placing impurities in a metallic environment using a tight-binding method, with a highly simplified model for the electronic structure consisting of a single s-band treated within the second moment approximation. He found that the impurity atom weakened the neighbouring metal–metal bonds. This is in agreement with Briant and Messmer's results.

For various reasons we consider Messmer and Briant's analysis to be highly questionable. Firstly, it is important to note that they did not calculate energies, only charge densities, from which bond strengths were inferred. Secondly, they used only very small

clusters of atoms for which the results could be quite different from the bulk. In particular the efficient screening in bulk metals is not properly reproduced in small clusters. Finally, the spherical approximation to the potential around each atom used in the work of Briant and Messmer is not appropriate for calculations on structures such as small clusters where there is highly directional bonding. In the case of Sayer's calculations the model used for the electronic structure was probably over simplified, a view supported by the work of Saqi and Pettifor (1987).

There is evidence against the decohesion model as proposed by Messmer and Briant. In the tight-binding calculations of Saqi and Pettifor (1987) bond energies were evaluated for different band fillings of the metallic host, which served to model the effect of different host metals. For a particular impurity these calculations showed additional cohesion and decohesion as the band filling of the metallic host was altered, implying that the electronegativity difference between the impurity atom and the host metal is not sufficient to determine even the sign of changes in cohesive energies. Saqi and Pettifor rationalised their results by saying that if charge was withdrawn from anti-bonding orbitals cohesion would be increased, but if charge was withdrawn from bonding orbitals cohesion would be reduced. This conclusion is entirely consistent with what is known about bonding in bulk transition metals. The binding energy does not increase monotonically across a transition metal series as the valency increases. Initially the binding energy increases as more and more electrons are added to bonding orbitals, then once the d shell has become half full, the extra electrons start filling anti-bonding orbitals producing a decrease in the binding energy. Applying this to the embrittlement problem we might expect that the withdrawal of electronic charge from nickel–nickel bonds by, for instance, the presence of a nearby sulphur atom would increase the cohesion of the nickel–nickel bonds since the 3d shell of nickel is more than half full.

A further interesting feature of decohesion models of embrittlement is their concentration on bond breaking processes, whilst completely ignoring processes involving atomic rearrangement. There is little doubt that a full theory of embrittlement will have to consider cleavage and shear on an equal footing, as in the work of Kelly, Tyson and Cottrell (1967), and Rice and Thomson (1974), a point which has been emphasised in the work of Eberhart *et al* (1984, 1985).

In summary, the question as to whether decohesion or increased cohesion occurs in embrittled systems is entirely open. If decohesion is demonstrated then it remains to be seen whether its occurrence can account for impurity-promoted intergranular embrittlement in real systems.

4. The bond mobility model of intergranular embrittlement

Haydock (1981) has suggested an alternative to the decohesion model of embrittlement which we shall call the bond mobility model. The central idea is that an embrittling impurity inhibits atomic rearrangement at a crack tip, which in turn inhibits the production of disclocations and thereby facilitates brittle fracture. It is presumed that the induced change in the ease of cleavage, due to the presence of an embrittling impurity, is a lesser effect.

A decrease in the ease of atomic rearrangement is said to occur when an embrittling atom forms bonds with the surrounding metal atoms that are of low mobility, as a result of which large forces are required to make the atoms slide over one another. At the atomic level the mobility of bonds is a consequence of their quantum mechanical nature.

In a metal electrons flow readily between the many unsaturated bonds, allowing atoms to break and reform bonds easily with their neighbours while undergoing an atomic rearrangement. This is ductility at the atomic level and it is this ease of atomic rearrangement which is suppressed by the presence of embrittling impurities. The low mobility of some metal-impurity bonds results from the formation of saturated bonds between the impurity atom and the host metal atoms, in contrast to the unsaturated bonds between metal atoms. In effect the embrittling impurities make the electron flow, and hence atomic rearrangement, less energetically favourable.

5. Our atomic model of a grain boundary

In this section we shall describe the choice of host metal and impurity elements, and the atomic model of a grain boundary, used in our work.

We chose aluminium to provide the metallic environment for our impurities, on the assumption that the most important feature of the host metal is its metallic nature. The commonly embrittled metals of most technological importance are the transition metals, which are primarily distinguished from aluminium by the inclusion of d-shell electrons. The reason for our choice of aluminium, a nearly-free-electron-like metal, was its relatively weak pseudopotential, which allowed us to perform calculations on relatively large unit cells. Due to the presence of valence d-shell electrons, the pseudopotentials of transition metals are strongly attractive, requiring a prohibitively large plane wave basis set with which to represent the potential and the wavefunctions.

The elements germanium and arsenic were chosen as representative embrittling impurities. Interestingly most embrittling elements are known to be from groups IV, V and VI of the periodic table, germanium and arsenic being from groups IV and V respectively. An important advantage of performing calculations with germanium and arsenic is that their atomic volumes are very close to that of aluminium. Consequently the degree of relaxation of the aluminium atoms surrounding the impurities is kept to a minimum and the effects that we see are due to the differences in electronic structure between the metal and the impurity atoms and not to the effects of volume mis-match. By relaxing the atomic positions for some test cases we found the relaxation to be negligible for the cleavage calculations, but significant for the shear calculations. Because of this the cleavage calculations described in section 7 did not include any atomic relaxation, while the shear calculations described in section 8 did include limited relaxation as will be discussed later.

The model grain boundary we have used in our calculations is essentially a close-packed layer of metal atoms doped with a one third concentration of substitutional impurity atoms, sandwiched between two slabs of pure metal. The close-packed layer was chosen in order to simplify the fracture calculations, fracture at the close-packed layer resulting in a high symmetry [111] surface. The aluminium [111] surface is known, both from experimental observations (Nielsen and Adams 1982), and theoretical calculations (Needs 1987), to undergo an extremely small degree of atomic relaxation. We found that we could get a reasonable separation between adjacent impurities in the close-packed layer, without increasing the size of the unit cell to unmanageable proportions, by substituting an impurity atom for every third aluminium atom. The impurity doped layer is illustrated in figure 3.

6. The pseudopotential total energy technique

For a detailed explanation of the pseudopotential method, as well as a review of recent calculations, the reader is referred to the paper by Ihm *et al* (1979). In the following we

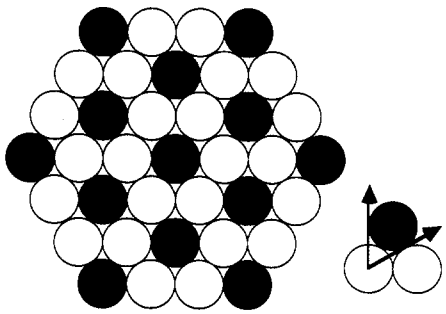

Figure 3. The idealised grain boundary, consisting of a close-packed layer of metal atoms (unfilled circles) doped with a one-third concentration of substitutional impurity atoms (filled circles). Two unit cell translation vectors are indicated, the third translation vector is perpendicular to the plane of the paper.

briefly describe the method with particular emphasis placed on numerical errors and the pseudopotentials used.

We calculated the total energies of periodic structures with large unit cells of atoms. The calculations were performed within a local density functional scheme with pseudopotentials used to represent the effect of the ion cores on the valence electrons, and the valence electron states represented by a finite plane wave basis set. Local pseudopotentials were used in order to speed up the calculations and allow the construction of large unit cells. The local density equations were solved self-consistently using matrix diagonalisation techniques in reciprocal space. The diagonalisations for the earliest calculations were performed with the approximate Löwdin perturbation method (Löwdin 1951) whilst later calculations used an exact and faster method recently developed by Nex (Nex 1987, Hodgson and Nex 1989). The integrations over the Brillouin zone were approximated by sampling on a regular mesh of points in reciprocal space following the method of Monkhorst and Pack (1976). Exchange–correlation terms in the local density equations and in the total energy were evaluated using the Ceperley–Alder form (Ceperley and Alder 1980, Perdew and Zunger 1981) of the local density approximation (LDA).

The three numerical sources of error in the total energy are: (1) truncation of the basis set after a finite number of plane waves, (2) approximation of the Brillouin zone integrals by finite sums and (3) lack of absolute convergence in the self consistent solution of the local density equations. Approximation (1) was tested by performing calculations on a variety of grain boundary structures using five different basis sets containing all plane waves with kinetic energy less than 4.5, 6, 6.5, 7 and 7.5 Hartree. We estimated that the 7 Hartree basis set energy cut-off used in our final calculations led to a numerical uncertainty in the energy differences between structures of less than 0.03 eV per unit cell for the eighteen atom unit cells (section 7) and less than 0.02 eV per unit cell for the nine atom unit cells (section 8). The largest calculations included up to two thousand plane waves. Approximation (2) was tested by performing calculations with four reciprocal space meshes, each having a different point density. On the basis of these calculations we selected a $4 \times 4 \times 2$ regular mesh for use with the unit cells containing eighteen atoms (section 7), giving an estimated uncertainty in the total energies of about 0.02 eV per unit cell, and a $4 \times 4 \times 4$ regular mesh for use with the nine atom unit cells (section 8), giving an uncertainty in the energies that was estimated to be about 0.01 eV per unit cell. Approximately (3) was dealt with by repeatedly solving the local density equations with successively better approximations to the potential obtained by quasi-Newton methods. The numerical uncertainty in the total energy due to incomplete self-consistency was estimated to be less than 0.0001 eV per unit cell and thus was insignificant in comparison to the first two sources of numerical error.

Table 1. The parameters of the modified local Heine–Abarenkov pseudopotentials. All quantities are in Hartree atomic units.

	Q_0	R	A	q_c	Z
Al	1.3900	1.150	0.1107	3.5	3
Ge	1.5000	1.120	0.5555	4.5	4
As	1.6633	1.085	1.3853	3.7	5

Table 2. Calculated and experimental values of the bulk moduli, in units of Mbars.

	Al	Ge	AlAs
Calculated	0.79	0.71	0.72
Experimental	0.74[a]	0.77[b]	0.77[c]

[a] Gschneider (1964)
[b] Landolt–Börnstein (1982).
[c] Cohen (1985).

The local pseudopotential used to represent the aluminium, germanium and arsenic ions was a modified form of the local Heine–Abarenkov type (Cohen and Heine 1970). In real space the Heine–Abarenkov pseudopotential is constant with a value $-A$ inside a core region of radius R. Outside the core region it has the value $-Z/r$, where Z is the valence of the element, and r is the radial distance from the nucleus. Fourier transforming the potential we obtain, in Hartree atomic units,

$$V(q) = -(4\pi/\Omega q^2)[(Z - AR)\cos(qR) + (A/q)\sin(qR)] \tag{1}$$

where Ω is a normalisation constant which we take to be the volume of the unit cell. The discontinuity at the core radius leads to spurious oscillations in $V(q)$. To ensure rapid convergence of the plane wave expansion for $V(q)$ we multiplied $V(q)$ by a function $f(q)$ which goes to zero at large wave-vectors. For the function $f(q)$ we chose the following form,

$$f(q) = \exp[-(q/q_c)^6] \tag{2}$$

which is a smoothed step function with a step at q_c. The parameter q_c was set to be approximately equal to the wave-vector where the second zero of $V(q)$ occurs. To ensure that our pseudopotentials accurately reproduced the properties of the corresponding atoms we constrained the first zero of $V(q)$ to be equal to the value tabulated by Cohen and Heine (1970), which we shall denote by Q_0. Keeping the value of Q_0 fixed leads to the condition

$$A = Q_0 Z/(Q_0 R - \tan(Q_0 R)). \tag{3}$$

This prescription leaves one free parameter which we took to be the core radius R. For each potential we adjusted R to fit the calculated lattice constants of pure aluminium, germanium and aluminium arsenide to the experimental values (4.02 Å, 5.62 Å and 5.62 Å respectively). The fitted parameters are given in table 1. We tested the pseudopotentials by calculating the bulk moduli, binding energies and some phonon frequencies of aluminium, germanium and aluminium arsenide. The values obtained are given in tables 2, 3 and 4 respectively and, for comparison, we include some values

Table 3. Calculated and experimental binding energies. Values calculated with our local pseudopotentials and with norm-conserving pseudopotentials are listed for comparison. Energies are in units of eV per atom for aluminium and germanium, and eV per pair of atoms for aluminium arsenide.

	FCC Al	Dia Ge	Zincblende AlAs
Calc. (local)	3.68	5.31	8.83
Calc. (norm-conserving)	3.67[a]	4.50[b]	8.2[c]
Expt.	3.40[d]	3.85[e]	7.7[f]

[a] Lam and Cohen (1982). [b] Needs (1989). [c] Ihm and Joannopoulos (1981).
[d] Brewer. [e] Moore (1949). [f] Wagman *et al* (1968).

Table 4. Calculated and experimental phonon frequencies in units of 10^{13} radians per second.

	FCC Al		Dia Ge		Zincblende AlAs	
Mode	L (X)	T (X)	TO (Γ)	TA (X)	TO (X)	TA (X)
ω_{calc}	5.68	3.11	5.64	1.35	5.86	1.80
ω_{exp}	6.08[a]	3.65[a]	5.73[b]	1.51[b]	6.30[b]	2.05[b]

[a] Stedman and Nilsson (1966) [b] *Landolt–Börnstein* (1982).

calculated using more accurate norm-conserving pseudopotentials (in table 3) and the experimentally determined values (in tables 2, 3 and 4). These results show that there is generally very good agreement between the values calculated with our local pseudopotentials and those calculated with the more accurate norm-conserving pseudopotentials and also reasonable agreement between the pseudopotential results and experiment. In addition Gillan (1989) has calculated the formation energy for a vacancy in aluminium using our pseudopotential and obtained excellent results. It is thought that the main source of error in the results obtained with norm-conserving pseudopotentials is the use of the local density approximation for the exchange-correlation energy and not errors inherent in the pseudopotential approximation.

7. The cleavage calculations

In this section we describe calculations we have performed on the cleavage of a pure and an impurity-doped aluminium crystal.

We studied the effect of an impurity on the ease of bond breaking by introducing a crack into our model system and calculating the energy as a function of the crack width. In order to simplify the calculations and their interpretation as much as possible we studied a simple crack formed by stretching the inter-layer bonds on either side of an impurity-doped layer. This crudely models the localised character of the strain in the region of a crack tip, although our crack has no tip, since the 'sides' of the crack are parallel. Initially, at small values of the tensile strain, the impurity-doped layer will sit in a position mid-way between the aluminium slabs on either side. At the point of fracture the impurity doped layer moves from the central position in order to bond preferentially with one of the aluminium slabs. At this point the crack opens catastrophically.

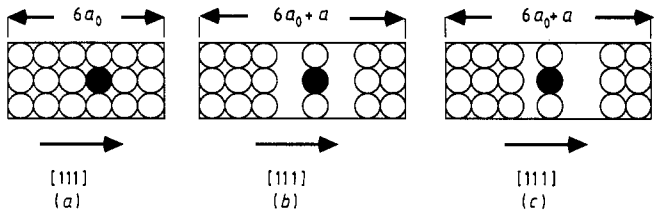

Figure 4. The unit cells used in the calculations of cleavage stresses. The open circles are aluminium atoms and the shaded circles are impurity atoms. The energy required to inhomogeneously strain the cell by a length a along the [111] axis is the difference between the energies of the two unit cells shown in (a) and (b). In (c) the impurity doped layer has been displaced from its central position by $a/8$.

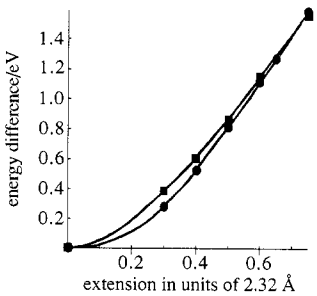

Figure 5. The energy versus extension, a, for pure aluminium (circles) and for arsenic-doped aluminium (squares). The energy is calculated as the difference in energy between the two unit cells depicted schematically in figures 4(a) and 4(b).

The maximum sustainable tensile stress was obtained from the gradient of the energy-extension curves at the point of fracture. Two sets of calculations were performed, one with an arsenic-doped impurity layer and one with a pure aluminium layer, both layers being in the central position (figure 4(b)). The point of fracture was defined as the largest extension at which the pure aluminium or arsenic-doped impurity layer still favoured the central position. The unit cells used for the cleavage stress calculations are shown schematically in figure 4. The unit cell shown in figure 4(a) is an unstrained cell consisting of six close-pacled layers, each of three atoms. The atomic positions in this structure are those of a perfect face-centred cubic lattice.

In figure 4(b) the inter-layer bonds between the impurity-doped layer and its immediate neighbours are stretched by a distance $a/2$, the net extension of the unit cell is thus a. The unit cell shown in figure 4(c) is identical to that shown in figure 4(b) except that the impurity-doped layer has been displaced a distance $a/8$ from its central position. We estimated the point of fracture by finding the value of a at which the energies of the two unit cells in figure 4(b) and figure 4(c) were equal. We plot, in figure 5, the energy difference between the unit cells shown in figures 4(a) and 4(b) against the extension, a, with circles and squares denoting the pure aluminium and the impurity-doped aluminium cases respectively. The slopes of the calculated energy-extension curves (figure 5) rise slowly around the point of fracture, which we estimated to be at an extension of $0.4\,a_0$ in both cases where $a_0 = 2.32$ Å and is the equilibrium spacing between layers. The gradients of the curves at the points of fracture are 1.2 eV Å^{-1} for pure aluminium and 1.0 eV Å^{-1} for arsenic-doped aluminium, for cracks of the area of three atoms. These correspond to cleavage stresses of 92 kbar and 79 kbar respectively. Thus the presence of the dilute layer of arsenic impurities reduced the cleavage stress of aluminium by approximately 14%.

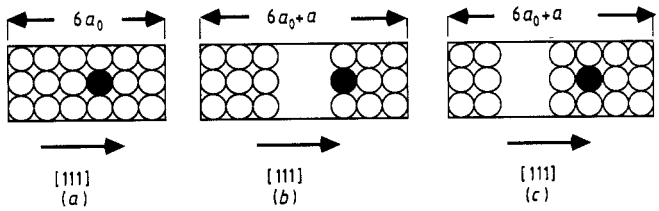

Figure 6. Schematic depiction of the unit cells used for the calculations of cleavage energies. The unit cell contains six [111] layers with three atoms in each layer. The open circles are aluminium atoms and the filled circles impurity atoms. (*a*) Unfractured sample, (*b*) Fractured at the impurity-doped layer. (*c*) Fractured one layer away from the impurity-doped layer.

The cleavage energies for our system were obtained by calculating the energy change on introducing a vacuum gap between two adjacent close-packed layers. A gap width of one and a half inter-layer spacings (3.48 Å) was found to approximate adequately an infinite vacuum gap. The unit cells used for these calculations are shown in figure 6. Cleavage energies were calculated for fracture both at the impurity-doped layer and one layer into the metal on either side of the impurity-doped layer in order to test for both first and second layer decohesion. Figure 6(*a*) schematically depicts the unfractured material. Figure 6(*b*) shows the material fractured at the impurity-doped layer and figure 6(*c*) shows the material fractured one layer into the metal. The energy for cleavage at the impurity-doped layer is given by the difference in energy between the unit cells shown in figures 6(*a*) and 6(*b*), while the energy for cleavage one layer into the metal is given by the difference in energy between the unit cells shown in figures 6(*a*) and 6(*c*). The results for pure aluminium, arsenic-doped aluminium and germanium-doped aluminium are given in table 5. These demonstrate that the inclusion of either germanium or arsenic impurities produces an increase in the inter-layer cohesion both at the impurity-doped layer and one layer into the metal, with percentage increases in the fracture energy of 8% and 4% respectively for arsenic impurities, and 1% and 5% respectively for germanium impurities.

8. The shear calculations

In this section we describe our calculations of the ideal shear stress for a perfect aluminium crystal and for an impurity-doped crystal.

Our aim was to calculate the effect of impurity atoms on the ease of atomic rearrangement of otherwise pure aluminium. A simple shear was applied to a sample of metal

Table 5. Cleavage energies, E_γ, for pure and for impurity-doped aluminium calculated as the difference in energy between the unit cells of figure 6(*a*) and figure 6(*b*) or (*c*) where E_a denotes the total energy per unit cell of the structure shown in figure 6(*a*), etc. Hence E_γ is the energy to create a crack of area equal to 3 atoms or 21.0 Å^2.

Impurity	E_γ (eV)
Al	$E_a - E_b = 1.80$
As	$E_a - E_b = 1.94$
As	$E_a - E_c = 1.88$
Ge	$E_a - E_b = 1.82$
Ge	$E_a - E_c = 1.89$

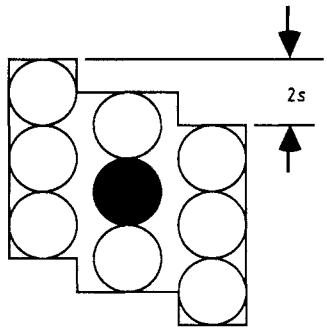

Figure 7. The unit cell, consisting of three close-packed layers, used in the calculations of shear stresses. Open circles are aluminiium atoms and shaded circles are impurity atoms. The first and third layers on either side of the central layer are rigidly displaced by a distance s and $-s$ respectively in the direction of second nearest neighbours in the close-packed layer. At each value of s the energy was minimised by relaxing the perpendicular separation of the first and third layers from the central layer.

and the corresponding energy changes calculated, both with and without an impurity concentration. Our geometry consisted of a unit cell containing three close-packed layers, shown schematically in figure 7, with the central impurity-doped layer, which is illustrated in figure 3, being identical to that used in the cleavage calculations. On either side of the impurity-doped layer we placed a close-packed layer of aluminium atoms giving a unit cell containing nine atoms. The two pure aluminium layers were slid distances s and $-s$ respectively, in the direction of second nearest neighbours within the close-packed layer. For each value of s we found that it was necessary, in order to minimise the total energy, to relax the perpendicular separation of the impurity layer from the adjacent aluminium layers on either side. The change in the perpendicular separation of the layers upon relaxation is denoted by b.

The results of the shear calculations are shown in figure 8. In figures 8(a), 8(b) and 8(c) we have plotted the energies of the sheared structures against the displacement, s, both before and after relaxation with respect to b (denoted by squares and circles respectively). All energies are in units of eV per unit cell whilst the displacements are in units of 1.64 Å (this unit was used because it is the shear displacement needed to create a stacking fault between two close-packed layers). We estimate that the maximum gradients of the relaxed energy-shear curves are 0.18 eV $Å^{-1}$ for pure aluminium, 0.23 for germanium-doped aluminium and 0.29 eV $Å^{-1}$ for arsenic-doped aluminium. The corresponding critical shear stresses are 24 kbar, 30 kbar and 38 kbar respectively. Thus the increases in the critical shear stress due to the inclusion of germanium and arsenic

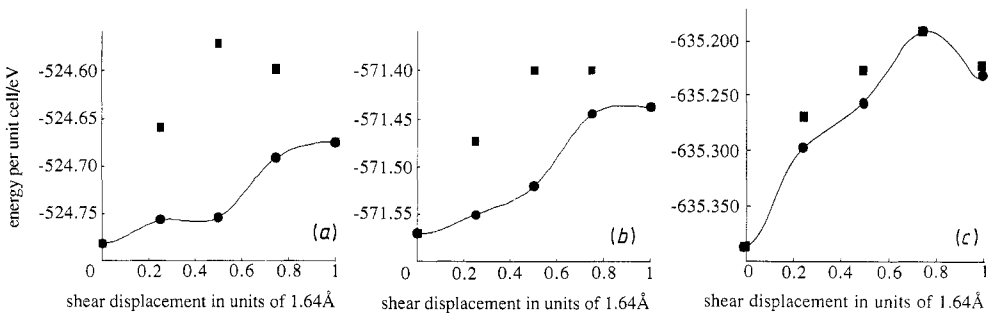

Figure 8. The results of the shear calculations, (a) for the pure aluminium structure, (b) for the germanium-doped structure and (c) for the arsenic-doped structure. The energy of the unit cell shown in figure 7 is plotted against the shear displacement s. The squares and circles are the energies before and after relaxation of the separation between the central layer and those on either side of it.

atoms are approximately 25% and 58% respectively. The associated shear energy barriers, defined as the difference between the largest and smallest energies for a given $E(s)$ curve, are 0.10 eV, 0.12 eV and 0.19 eV respectively.

The degree of relaxation during the shear process was also very different in each case. For pure aluminium the relaxation was large, reaching a maximum value of $b = 0.035$ Å for a shear displacement of $s = 0.82$ Å. The maximum relaxation for the arsenic-doped case was about one half of this value whilst the magnitude of the relaxations for germanium were intermediate between those for pure aluminium and arenic-doped aluminium.

9. Conclusions

In this section we discuss the deocohesion and bond mobility models of embrittlement in the light of our results.

We have described in preceding sections the decohesion model of embrittlement and a set of fracture calculations that we have performed in order to test the model. The decohesion model asserts that an impurity which is more electronegative than the host metal will reduce inter-layer cohesion by drawing charge onto itself at the expense of surrounding metal bonds, and that the change in cohesion is correlated with the change in the maximum sustainable tensile stress. The results of our fracture calculations showed consistently that neither germanium nor arsenic impurities reduced the fracture energy, in fact both impurities were found to increase cohesion, though not by particularly large amounts, both at the impurity-doped layer and one layer away. In addition the arsenic impurities reduced the maximum sustainable tensile stress (tensile stress calculations with germanium were not performed). This is contrary to the decohesion model as both arsenic and germanium atoms are more electronegative than aluminium, both increased the cohesion, and the change in the maximum sustainable tensile stress was not directly correlated with the change in the cohesion. We conclude that the decohesion model does not correctly describe the impurity induced changes in bonding in our model system and we see no reason to believe that it will give correct predictions in other systems.

In order to study fracture we had to reduce the problem down to what we consider to be the two fundamental underlying processes, bond breaking and atomic rearrangement. By performing cleavage calculations (section 7) we found that arsenic impurities reduced the maximum sustainable tensile stress, which we referred to as the cleavage stress, by some 14%, with fracture occurring at the same value of the strain in both the doped and undoped cases. The effect of the arsenic impurities was to increase the ease of bond breaking. In addition, the slope of the energy-extension curve at small extensions was increased by the presence of the impurities, an effect which we suggest is an indication of reduced bond mobility. The effect of the impurities on the ease of atomic rearrangement can be seen more clearly from the results of the shear calculations (section 8). Comparing the results for the shear of the three systems without relaxation of the inter-layer separation (filled squares in figures 8(*a*)–8(*c*)) we see that the curves for all three cases are, perhaps somewhat surprisingly, very similar; the shear stress and the associated energy barrier (the maximum increase in the energy during shear) are qualitatively the same in all three cases. Relaxation of the inter-layer spacings produced dramatically different effects depending on whether impurities were present or not. The arsenic-doped structure was unable to reduce its energy to any significant degree by atomic relaxation, whereas the pure aluminium structure was able to reduce its energy

by a very large amount. Interestingly, given that germanium is seen experimentally to be a weaker embrittler than arsenic, the results with germanium impurities were intermediate between the results for the pure structure and the arsenic-doped structure. Clearly the major effect of both impurities on the host metal was to inhibit atomic rearrangement. The results of the cleavage and shear calculations are consistent with the bond mobility model of embrittlement. Following the line of argument proposed by Haydock (1981), and elaborated upon in section 4, we suggest that arsenic impurities inhibit ductile fracture by impeding crack tip dislocation emission, whilst aiding brittle fracture by increasing the ease of cleavage at the crack tip.

Our approach to determining bond mobilities has been to calculate the stress required to initiate well defined atomic rearrangements in our model system. It would be desirable to try to determine the mobility of bonds directly by performing a single electronic structure calculation on a system. One possibility is that replacing a metal atom with an impurity atom might reduce, in the region around the impurity, the local density of states close to the Fermi energy. Atomic rearrangement would then require a transfer of electrons to rather high energy states, leading to a high energy barrier and associated stress. This is consistent with the observation that insulators, which have a vanishing density of states at the Fermi energy, fail by brittle fracture, though whether there is sufficient information in the local density of states near the Fermi energy to determine the mobility of bonds is currently unknown.

10. Summary

In summary, we have studied impurity-promoted intergranular embrittlement by considering the effect of segregated impurities on two fundamental processes, the change in the ease of bond breaking, and the change in the ease of atomic rearrangement. The changes in the ease of bond breaking and the ease of atomic rearrangement were determined by performing simple shear and fracture calculations with idealised geometries. We found that a dilute layer of substitutional arsenic impurities reduced considerably the ease of simple shear and increased, to a lesser extent, the ease of simple fracture in otherwise pure aluminium. In addition arsenic impurities were found to strengthen the inter-layer cohesion, both at the first layer and the second layer. The effect of germanium impurities on the strength of inter-layer cohesion and the ease of shear was similar to that of arsenic though the changes were less pronounced. These results cast doubt upon the decohesion model of embrittlement, whereas the bond mobility model of embrittlement is entirely consistent with our results. Our results show that both germanium and arsenic impurities reduce the ease of atomic rearrangement and that arsenic impurities increase the ease of bond breaking (bond breaking calculations with germanium impurities were not performed). We suggest that these effects suppress ductile processes and favour brittle fracture.

Acknowledgments

We would like to thank Professor R Haydock for interesting discussions and his kind hospitality while two of us (LG and RJN) visited the University of Oregon during the course of this work. We also thank Dr A J Sutton for helpful conversions. The computations were performed with the use of the Cray X-MP/48 facility at the San Diego

Supercomputer Centre. This research was supported by the Science and Engineering Research Council (SERC) and by the US National Science Foundation (NSF) under Grants No Condensed Matter Theory DMR-8122004 and No INT-8402918.

References

Brewer L *Lawrence Berkeley Laboratory Report No* 3720 (unpublished)
Briant C L and Messmer R P 1980 *Phil. Mag.* B **42** 569
Ceperley D M and Alder B J 1980 *Phys. Rev. Lett.* **45** 566
Cohen M L 1985 *Phys. Rev.* B **32** 7988
Cohen M L and Heine V 1970 *Solid State Physics* vol 24 (New York: Academic) p 47
Eberhart M E, Johnson K H and Latanision R M 1984 *Acta Metall.* **32** 955
Eberhart M E, Latanision R M and Johnson K H 1985 *Acta Metall.* **33** 1769
Gillan M J 1989 *J. Phys.: Condens. Matter* **1** 689
Goodwin L, Needs R J and Heine V 1988 *Phys. Rev. Lett.* **60** 2050; *Phys. Rev. Lett.* **61** 133
—— 1989 *Europhys. Lett.* **9** 551
Gschneider K A 1964 *Solid State Physics* vol 16 (New York: Academic) p 276
Haydock R 1981 *J. Phys. C: Solid State Phys.* **14** 3807
Hodgson M J and Nex C M M 1988 *J. Comput. Phys.* **79** 484
Ihm J 1988 *Rep. Prog. Phys.* **51** 105
Ihm J and Joannopoulos J D 1981 *Phys. Rev.* B **24** 4191
Ihm J, Zunger A and Cohen M L 1979 *J. Phys. C: Solid State Phys.* **12** 4409
Kawabatta T, Suenga H and Izumi O 1984 *J. Mater. Sci.* **19** 1007
Kelly A, Tyson W R and Cottrell A H 1967 *Phil. Mag.* **15** 567
Landolt-Börnstein, Numerical Data and Functional Relationships in Science and Technology 1982 Group 3, vol 17, subvol a, ed O Madelung (Berlin: Springer)
Lam P K and Cohen M L 1982 *Phys. Rev.* B **24** 4224
Losch W 1979 *Acta Metall.* **27** 1885
Löwdin P O 1951 *J. Chem. Phys.* **19** 1396
Messmer R P and Briant C L 1982 *Acta Metall.* **30** 457
Monkhorst H J and Pack J D 1976 *Phys. Rev.* B **13** 5188
Moore C E 1949 *Atomic Energy Levels* NBS Circular No 467, vol 1 (Washington, DC: US Government Printing Office)
Needs R J 1987 *Phys. Rev. Lett.* **58** 53
—— 1989 to be published
Nielsen H B and Adams D L 1982 *J. Phys. C: Solid State Phys.* **15** 615
Nex C M M 1987 *Comput. Phys.* **70** 138
Ogura T, McMahon C J, Feng H C and Vitek V 1978 *Acta Metall.* **26** 1317
Painter G S and Averill F W 1987 *Phys. Rev. Lett.* **58** 234
Perdew J and Zunger A 1981 *Phys. Rev.* B **23** 5048
Rice J and Thomson R 1974 *Phil. Mag.* **29** 73
Saqi M A S and Pettifor D G 1987 *Phil. Mag. Lett.* **56** 245
Sayers C M 1984 *Phil. Mag.* B **50** 635
Stedman R and Nilsson G 1966 *Phys. Rev.* **145** 492
Thomson R 1986 *Solid State Physics* vol 39 (New York: Academic) p 58
Troiano A 1960 *Trans. ASM* **52** 75
Wagman D D *et al* 1968 *National Bureau of Standards Technical Note* vol 270 (Washington, DC: US Government Printing Office) p 3
Wert J A and Lumsden J B 1985 *Scr. Metall.* **19** 205